IMAGE DEGRADATION DUE TO DIFFRACTION, REFLECTION AND SCATTERING IN AN OPTICAL SYSTEM

by

Jerome A. Zadnik

Thesis submitted to the faculty of the
Virginia Polytechnic Institute and State University
in partial fulfillment of the requirements for the degree of

MASTER OF SCIENCE

in

ELECTRICAL ENGINEERING

APPROVED:

R.O. Claus, Chairman

T.C. Poón

R.J. Pieper

April, 1987

Blacksburg, Virginia

IMAGE DEGRADATION DUE TO DIFFRACTION, REFLECTION AND SCATTERING IN AN OPTICAL SYSTEM

by

Jerome A. Zadnik

Committee Chairman: Richard O. Claus
Electrical Engineering

(ABSTRACT)

The focal plane power distribution due to a bright source is analyzed for an infrared imaging optical system. Irradiance from the bright source is spread throughout the focal plane according to the characteristics of the system. This effect is attributed to diffraction, reflection and scattering in the optical train. Expected focal plane power distributions due to diffraction and multiple reflections between dielectric surfaces are calculated and compared to measured data. The difference is attributed to scatter characteristics of the optical elements. A brief overview of the major sources of scatter lays groundwork for a further analysis of scattering characteristics in the optical system.

1.0 INTRODUCTION

Optical systems are sometimes required to detect an object in close proximity to a bright source such as the sun or a laser. Ideally, optical radiation from a source will be limited to a small region on the focal plane. However, in a typical infrared imaging system, a small amount of incident power is spread over the entire focal plane. With a bright source, this may produce a prominent effect, capable of washing out the image and obscuring the object of interest.[1] A synchronized short pulse technique is used to provide a means of mapping the power distribution on the focal plane as a function of field of view angle. Until now, specific factors that compose the distribution of incident power on the focal plane have not been investigated. An analysis is presented here to effectively separate the contributions of diffraction, reflection and scatter in the optical system from the measured data.

The effects of diffraction on the focal plane power distribution was computed through the implementation of a computer aided analysis. Energy reflected at optical interfaces create ghost images through the optical system. The amount of energy that arrives at the focal plane from these multiple reflections in the optical train is calculated with the assistance of CODE V optical design program. It is found that diffraction has a minimal effect, but the reflected power can be a significant contributor to the measured data in certain field of view positions. The remainder of the data is attributed to scattering in the system. It has not yet been determined exactly where the scattering originates, however, many sources can be included in a future scatter analysis.

2.0 OPTICAL SYSTEM DESCRIPTION

This analysis was done on an opto-mechanical thermal imaging sensor. Using a small array of Mercury Cadmium Telluride (HgCdTe) detectors, it responds to optical radiation with wavelengths between eight and twelve microns. The detectors examine the field of view in a serial scan format, allowing the system to easily interface with an ordinary television monitor. Utilizing a simple optical design, this sensor also lends itself to a clear analysis. The optical train consists of only six elements: a front window, two scan mirrors, a single focussing lens and a dewar window behind which the small array of detectors are arranged. The front window is a zero power germanium lens with anti-reflection (AR) coated surfaces to reduce reflection losses. The serial scan format is obtained with the use of a rotating multifaceted horizontal scan mirror and a vertical scanning paddle mirror. The multifaceted mirror has a diamond turned aluminum surface, and the paddle mirror consists of an evaporated gold coating on a germanium substrate. The paddle mirror serves as the aperture stop which is located directly in front of the only focussing element in the optical train. This coated germanium lens concentrates the infrared radiation through a flat zinc selenide (ZnSe) dewar window onto the cooled HgCdTe detectors. The mirrors effectively scan the detectors over the field of view. After calibration by known incident radiation, these detectors also provide the means with which to measure power density at the focal plane. Because this system does not contain elaborate focussing elements and complicated scanning mechanics, optical surfaces that contribute to reflection and scatter are minimized.

3.0 EXPERIMENTAL TECHNIQUES

A synchronized short pulse technique used here allows accurate measurement of focal plane irradiance. A simplified bench setup is shown in figure 3.1, which utilized a five watt CO_2 laser operating at 10.6 microns. Continuous wave output is pulsed with acousto-optic modulator, that is synchronized to the scanning mechanism of the imaging system. Laser pulses are spatially filtered, expanded and recollimated by an off axis parabolic mirror, providing a plane wave to flood the front aperture of the imaging sensor. The center portion of the gaussian intensity distribution is used in order to provide the plane wave with an amplitude distribution that is nearly constant. The arrangement results in a point source imaged at infinity. This is necessary in order to assure that the incident power is focussed down to one detector on the focal plane, for calibration purposes. The measurement sequence was as follows:

1. The laser source was precisely calibrated both in continuous wave and pulsed operation.

2. The detector postamp was chosen as a measurement point The electrical response at this point was then measured versus incident laser radiation and this calibration was used to determine the linear operating range of the system.

3. Field sync pulses were used to synchronize the laser output

to the scanning format. Duration of the pulse was approximately equal to six microseconds, which is less than one line scan of the TV monitor. This ensured that the system operated in its linear range under the same conditions as the system calibration. This also allowed more precise spatial information, because irradiance from every pulse would reach each detector, yielding its response to the current optical input. Data is available for many scan positions where the detectors are not saturated. A time delay between the scanner field pulse, and laser pulse was varied to obtain irradiance data that correspond to different positions over the entire focal plane.

4. The pulse technique allowed accurate measurement of the focal plane power distribution as a function of elevation angle in the vertical field of view of the imaging system.

Since the laser is pulsed at selected times during a scene scan, the laser beam will be focused onto the center of the focal plane while the detectors are located elsewhere. A map of the power distribution signals over the focal plane is determined by measuring the detector array output as a function of scanner displacement angle. By adjusting the laser power incident on the imaging system, the postamp output voltage can be maintained at a fixed value in the linear operating region for various scanner displacement angles. Measured power for various scan positions are normalized to the power level for a laser

pulse occurring at the center position, then plotted as a function of field of view (FOV) angle.

As an example, consider figure 4.1 which shows typical data with the laser positioned in the center of the FOV. A time delay between the FLIR field pulse and laser pulse was varied to move down the FOV center. As the time delay was changed, the laser power was adjusted to maintain the postamp output at 20 mV. The incident power was recorded versus FOV elevation, then normalized to the power level for the laser pulse corresponding to the center scan position.

4.0 OBSERVED EFFECTS

According to geometric optics, a constant amplitude plane wave incident on an ideal optical system is concentrated into a single bright spot on the focal plane. This is not precisely the case with real systems where the bright spot from a low power source usually exceeds the diffraction limited airy disk. Many factors can cause the bright region on the focal plane to be larger than the diffraction limit and may even be a desirable design parameter. For the infrared imaging system reported here, incident flux from the center of the FOV illuminates the entire focal plane. A close examination reveals that small amounts of optical radiation are separated from the main bundle and spread throughout the optical system. The intensity of the resulting power distribution on the focal plane falls off with distance from the center bright spot, so the irradiance at the edge of the FOV is orders of magnitude lower than the focal point. Even this small amount of radiation can be detected, and may cause problems particularly in

focusing higher power illumination.[2]

HgCdTe detectors used at the focal plane of the imaging system have a dynamic range of about five hundred. That is, the detector saturates at an incident power level five hundred times higher than is required for it's smallest response. Outside of this linear operating region, the detectors cannot respond to small changes in incident flux, resulting in no useful output. When a low intensity plane wave is incident on such a system, a bright spot is seen within a darker background. For example, a small blackbody radiator at 500°K placed a distance away from the infrared sensor resembles a point source and will appear as a small bright spot in the image. As the incident intensity is increased by a factor of five hundred, the scanning detectors saturate as they cross the center of the field of view, and the surrounding region is effected according to the focal plane power distribution. With a further increase in intensity, the detectors crossing the center are in hard saturation, and close to saturation in the surrounding region, leaving a large portion of the image effected by the incident flux. This of course can have a devastating effect on image regeneration and can render the system ineffective as an imaging device.

Using the pulse technique described above, a laser was placed in the center of the field of view and calibrated power density measurements were taken at points across the center of the focal plane. Data was normalized to the value at the center of the image, and is plotted on a semi-log plot in figure 4.1 as a function of vertical field of view angle. Coordinates are provided for vertical field of view angle in order to easily correlate the quantitative measurements of power

density distribution on the focal plane with what might be seen by the imaging system. Since the detectors have a dynamic range of only five hundred, this graph shows that the center of the field of view can have detectors in hard saturation when the outer edges are just beginning to be effected. Image degradation is obvious. With any detectors in saturation, there can be no information with which to reconstruct the image in that area. This effect results in the loss of information relating to an object in close proximity to a bright source.

5.0 OPTICAL SYSTEM ANALYSIS

Assuming that the measured data is due to diffraction, reflection and scattering, the optical system was analysed in terms of diffraction effects at the focal plane and reflection between optical elements. These calculations were compared to measured focal plane data in order to determine the largest contributor to the focal plane power distribution.

5.1 DIFFRACTION

Inherent in the wave nature of light, diffraction in the optical system may be the most obvious candidate for the energy spreading effect. The Fraunhofer or far-field diffraction pattern of a constant intensity plane wave incident on a lens or an optical system, is observed at the focal plane of the system. For a circular aperture, the intensity pattern is radially symmetric and is expressed in terms of a Bessel function.[3,4]

$$I = I_o\left[\frac{2J_1(ka\omega)}{ka\omega}\right] \qquad (5.1.1)$$

where $$\omega = \frac{r}{\sqrt{r^2 + d^2}}$$

and I_o is the intensity at the center of the pattern,

J_1 is a bessel function of the first kind of order one,

k is the wave number of the incident radiation,

a is the radius of the diffracting aperture,

r is the radial distance on the focal plane,

d is the distance from the diffracting aperture to the focal plane.

The intensity distribution of this pattern consists of a bright region in the center surrounded by concentric rings of lesser intensity. These surrounding rings fall off in magnitude with distance from the center, and theoretically extend to infinity. 91% of the irradiance is contained within the central region and the first bright ring.[4] The remaining 9% is spread over the rest of the focal plane and beyond. Because of the rapid intensity falloff with distance from the center, the power density at the edge of a small focal plane can be orders of magnitude below that at the center of the airy disk. The exact amount depends on the characteristics of the system in question. These features make diffraction a very attractive candidate as a possible cause of the measured data (figure 4.1).

Diffraction effects at the focal plane of a scanning optical system such as the one analyzed here are principally due to the entrance aperture of the system, and calculated according to equation (5.1.1). The scanning mirrors effectively serve as a mechanism to scan the detectors across the diffraction pattern of this aperture. Diffraction can also originate from the aperture stop of a scanning system and is dependant on the optical radiation incident on the stop itself. Consider the case in figure 5.1 where a laser is located in the center of the FOV of an imaging system, and the scan position corresponds to an off axis location. The primary diffraction pattern due to the entrance aperture is centered at the on-axis point where the laser radiation is focussed. Being off axis, the detector (as well as the aperture stop for this system) is exposed to an off-axis position that is directly related to the scan angle. The aperture stop then gives rise to a secondary diffraction pattern according to its incident intensity. Further difficulties arise from the presence of multiple apertures in the system which, for some cases have a significant effect in the far field diffraction pattern.[5,6] Software is available for a complete computer description of the diffraction effects in an optical system.[7] This would allow the calculation of elegant diffraction equations that become rather difficult when considering multiple apertures, tilted elements, and vignetting effects. However, before using this software, it was decided that a resonable approximation can be attained by neglecting the secondary effects of the aperture stop, and calculating the primary diffraction pattern of the front window on the focal plane. This result would be compared to the measured data to determine if more precise

considerations are required.

The entrance aperture is 4.216 cm in diameter, and 8.403 cm from the focal plane. The appendix describes the calculation of the normalized diffraction envelope for this configuration which is plotted as a function of focal plane position in figure 5.2. Comparison of the graph in figure 5.2 with the normalized power density distribution in figure 4.1 reveals that diffraction effects are approximately three orders of magnitude lower than the data measured at the focal plane. Accounting for only about one tenth of one percent shows that diffraction is a negligible contributor to the power spreading effect, giving little reason to pursue a further computer analysis.

It is cautioned that diffraction is highly dependant on the characteristics of the individual optical system and cannot be assumed negligible for all cases. Instead, an analysis is needed for each system, to determine it's contribution.

5.2 REFLECTION

Another possible contributor to the measured data in figure 4.1 is reflection in the optical system. A certain amount of reflection is characteristic of all dielectric interfaces. Incident light can be reflected and re-reflected between optical elements, some of which will find it's way to the focal plane. According to the Fresnel formulas, reflection is a function of incident angle, polarization and refractive index.[8] For near normal incidence, small angle approximations reduce these formulas to a single expression for reflected power as in equation (5.2.1).

$$P_r = I \frac{(n_1 - n_2)^2}{(n_1 + n_2)^2} \qquad (5.2.1)$$

where I is the power incident on the interface,

n_1 is the refractive index for the first medium,

n_2 is the refractive index for the second medium.

The irradiance on the focal plane due to reflection can be reduced by antireflection coatings on lenses and windows, but it cannot be entirely eliminated.

In view of the fact that an even number of reflections are required to reach the focal plane, only the second, fourth, sixth etc. are of interest. Assuming one percent reflection at a coated interface, optical radiation is reduced by a factor of 100 with each reflection. Consequently, the irradiance level corresponding to each successive even reflection is further reduced by a factor of 10^4. For this reason, only second reflections will be considered in this analysis.

An optical system that contains N transmissive elements has N(2N-1) possible interface combinations that will support second reflections. If detectors at the focal plane also reflect one percent of the incident power, then N(2N+1) combinations are possible. The optical system analyzed here has three transmissive elements, which support twenty one different reflections. For a radially symmetric optical system, each pair of reflections distribute a fraction of the incident power over a circular area of the focal plane. The size of each circle is a function

the curvature and position of the corresponding interface pairs. Focal plane irradiance results in superimposed concentric circles of differing intensity centered on the optical axis of the system.

A computer analysis was performed to calculate the radius of each circle and identify the corresponding surfaces. Exact reflectance values are unknown at this time, therefore assumptions were made for each interface. With a refractive index of 2.4 for Zinc Selenide, equation 5.2.1 indicates 17% of the incident power is reflected at each interface. Germanium, with a refractive index of 4.003, has an uncoated reflectance of 36%.[9] For this reason germanium elements in infrared sensors are usually coated. Discussions with manufacturers revealed that typical reflectance values of coated germanium elements range from, a few tenths of one percent to a few percent. For the preliminary analysis, all surfaces are assumed to be coated to a reflectance of one percent.

Results of the reflection analysis are shown in figure 5.3. The reflected power density values are normalized to the irradiance on the focal plane as if the radiation is focussed to, and evenly distributed over, a circular area the size of the airy disk. Results of the reflection analysis along with the calculated diffraction envelope is superimposed on the measured data in figure 5.4. This comparison shows that focal plane irradiance from second reflections approach the measured data near the edges of the FOV, and may be a significant factor contributing to this data. For this particular system, the calculated reflected power is 10^{-4} less than the measured data at the center, but the difference between the two curves becomes smaller as radial distance

from the center of the focal plane increases. At the edges, the reflected contribution accounts for about 35% of the total focal plane irradiance.

Although expected reflectance values are used in the optical system at this time, it is clear that reflection in the optical train may be a significant factor in but does not entirely explain the measured data.

5.3 OPTICAL SCATTERING

Calculations show that a small fraction of the measured data originates from diffraction through the entrance aperture of the system, and a larger portion is due to reflections between optical elements. The difference between the measured data and calculation may be attributed to scattering in the optical system itself. Several sources of scattering can contribute to the overall effect, most of which are predictable. They include bulk scatter along with scattering from the surface roughness, subsurface damage and contamination.

Lattice discontinuities and Rayleigh scatter constitute Bulk scatter which is inherent in the substrate of refractive elements, but is usually small for long wavelengths. Small cracks under the polished surface of a lens can remain from the rough grinding or diamond machining process as subsurface damage. Scatter from the random roughness of imperfect optical surfaces is a statistical effect, and has gained much attention. Lens and mirror contamination is difficult to control, and can increase the scattering characteristics of an optical element. All these factors add to scattered light received by the focal plane detectors, but an in-depth analysis is needed to identify their

relative contributions to the measured data.

5.3.1 SURFACE ROUGHNESS

Surface roughness scatter is related to the distribution of micro-irregularities characteristic of all optical surfaces. These are classified as optically smooth when the height of roughness on the surface is much smaller than a wavelength. However, scatter from microrough surfaces may effect the performance of a precision optical instrument.[13] The roughness typical of an optically smooth surface has a height less than a hundred angstroms, and exhibits random properties lending itself to a statistical analysis. Howevèr, diamond turned mirrors such as the horizontal scanning mirror, display a periodic component related to the diamond turning process which is superimposed on the typical random roughness.[14,15,16] Microrough optical surfaces can be considered as a Fourier series of superimposed sinusoidal diffraction gratings with differing periods, height and orientation.[15,16] Each grating diffracts or scatters light according to the grating equation:

$$a(\sin \Theta_i - \sin \Theta_d) = \lambda$$

where a is the spatial wavelength of the grating,

λ is the wavelength of incident radiation,

Θ_i = Angle of the incident light to the surface normal,

Θ_d = Angle of diffracted light to the surface normal.

Only first order diffraction is considered, because second order effects

can be neglected for this kind of surface.[16] This equation implies that smaller spatial wavelengths on the surface give rise to larger angle scattering, and larger spatial wavelengths cause scattering at angles close to the specular direction.

A number of methods are used to determine the profile of an optical surface.[17] Generally, profiles from arbitrary rough surfaces are described in terms of a spectral density function or in terms of correlation length along with rms height and slope. These expressions can in turn be related to scattering characteristics of the surface.[18] Scatter from certain optical elements can be measured directly, and is usually expressed in terms of a bidirectional reflectance distribution function (BRDF) or a bidirectional transmittance distribution function (BTDF) for mirrors and optical windows respectively.[19] The characteristic bidirectional distribution function of a measured optical element describes how incident radiation is scattered by that element. No such measurements have been done for the elements of the system described here. However, it is interesting to note that scatter measurements and theory agree well with surface topography,[15,17,18,20,21] indicating that scatter from a clean optical element is largely due to surface roughness.

5.3.2 SUBSURFACE DAMAGE

Small surface cracks are produced when generating optical components by grinding techniques or diamond machining. This damage is characteristic of cutting or grinding an element from a brittle substance.[10] Cracks produced by grinding are effected by many factors

and are described in terms of fractured and relief layers depicted in figure 5.5. The relief layer is what would be measured by a mechanical profiling instrument. It is the top layer of an element that has been chipped and broken to produce a rough topography on the surface. The fractured layer is immediately below the surface, and consists of cracks extending into the depths of the material. The size and propagation depths of these cracks are related to the speed and cut of the generating technique. However, the fractured layer is about four times that of the relief layer independent of the abrasive used.[11] Optimistically, these cracks are reduced or removed by the polishing process.

Damage in other monocrystalline materials were measured and compared to the damage in glass. The frayability criterion is the ratio of sheer resistance to the resistance of breakage. It was found that materials with a frayability criterion larger than one, including zinc selenide and germanium, also have a fractured layer about four times the thickness of the relief layer. A very fine surface is attained by grinding with successively finer grinding compounds before polishing. This is meant to remove most of the surface that was fractured by the compound in each previous run. The relief layer of a surface prepared in this way is about 300 angstroms before polishing, which means that surface damage extends to approximately 1500 angstroms below the surface. The polishing process creates a smooth layer of material on the order of about 500 angstroms over the entire surface. Even allowing for material removal during the polishing process, this may leave a significant fractured layer that is covered over by a smooth surface.

Subsurface damage such as this contributes to scattering according to the depth, orientation and extent of these micro-cracks. If polishing is done immediately after a rough grinding or diamond generating technique, the cracks can be much more extensive, adding significantly to element scatter.[12]

Methods of reducing or eliminating subsurface damage include gradual grinding techniques as well as super-polishing the surface. Super-polish methods may include polishing for an extended period of time or polishing and etching away the polished surface in cycles until the damage is eliminated.

5.3.3 CONTAMINATION

Surface contaminates such as dust, smoke, dirt and grease will give rise to scattering in an optical system. In view of the fact that it is hard to keep a surface clean, contaminates may be an additional factor to be considered in a scatter analysis.[22]

Upon visual inspection of the measured optical system, the top of the focussing lens was observed to be severely contaminated with a dark, grainy coating over the entire surface. Time limitations did not allow the system to be cleaned and remeasured. This contamination presumably increased the amount of total scattered light in the system.

The effects of opaque particles on the photometric properties of an optical surface has been studied for differing particle sizes, reflectivity and degree of contamination.[23] It was found that transmittance and scattering from a contaminated glass slide depends on the size and concentration, but not as much an the reflectance of the

particles. Scattering from a contaminated surface was integrated over the half space of 2 , collecting only forward scattering from a contaminated glass slide. The scattered light ranged from a few percent to eighteen percent of the incident light for varying particles and concentrations. A large portion of this may reach the focal plane due to the high peak in the BTDF at the specular direction.[24] With this large amount, contaminated surfaces may be a significant contributor to the overall scatter characteristics of an imaging system.

6.0 CONCLUSION

The analysis presented here is highly dependant on the individual optical system involved. The effects of diffraction and reflections are calculated for an infrared imaging system in order to isolate specific factors contributing to the power distribution on the focal plane. It was found that diffraction only accounts for a small fraction of the distribution. Reflection between refractive optical elements in the system seems to account for a larger percentage in certain areas, but does not entirely explain the measured data. The difference is attributed to many causes of scatter in the optical system. An in depth scatter analysis will be needed to identify the effects that have the highest contribution to scatter characteristics, so that specific factors can be pin pointed. It is expected that the focal plane power distribution in an imaging system can be reduced by improving these specific factors or by incorporating them into design considerations of future systems that include low scatter elements.

Several computer programs are available to calculate scattering from various surfaces including lenses and mirrors.[25] Off axis effects such as scattering from baffles and lens mounts are of interest as well.[26] This is the topic of continuing effort in an attempt to determine the causes of the focal plane power distribution in an optical system.

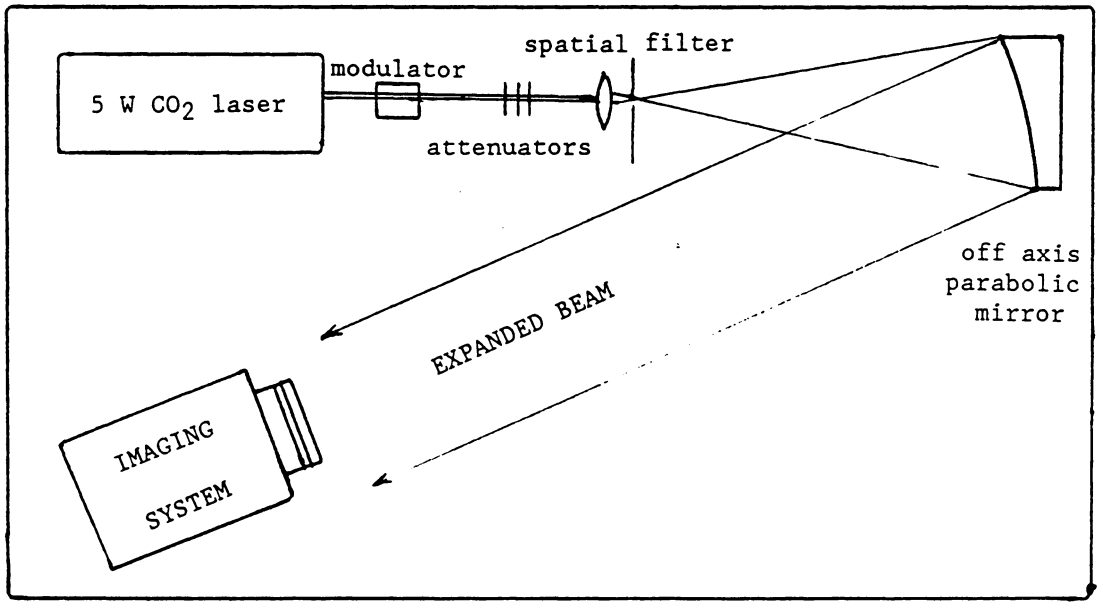

FIGURE 3.1 Simplified optical bench setup shown without power tap and monitoring elements.

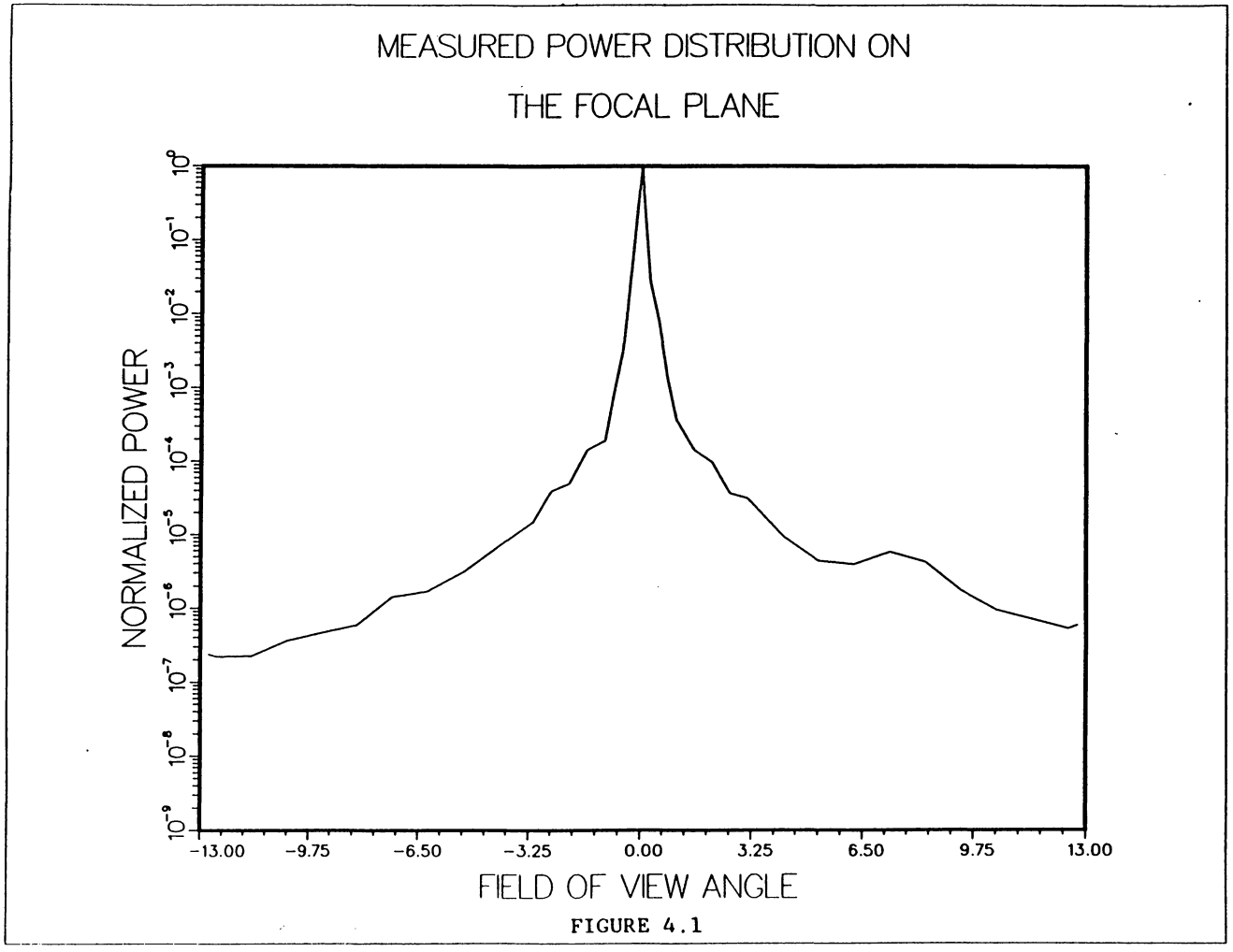
MEASURED POWER DISTRIBUTION ON
THE FOCAL PLANE
NORMALIZED POWER
10^{0}
10^{-1}
10^{-2}
10^{-3}
10^{-4}
10^{-5}
10^{-6}
10^{-7}
10^{-8}
10^{-9}
-13.00
-9.75
-6.50
-3.25
0.00
3.25
6.50
9.75
13.00
FIELD OF VIEW ANGLE

FIGURE 4.1

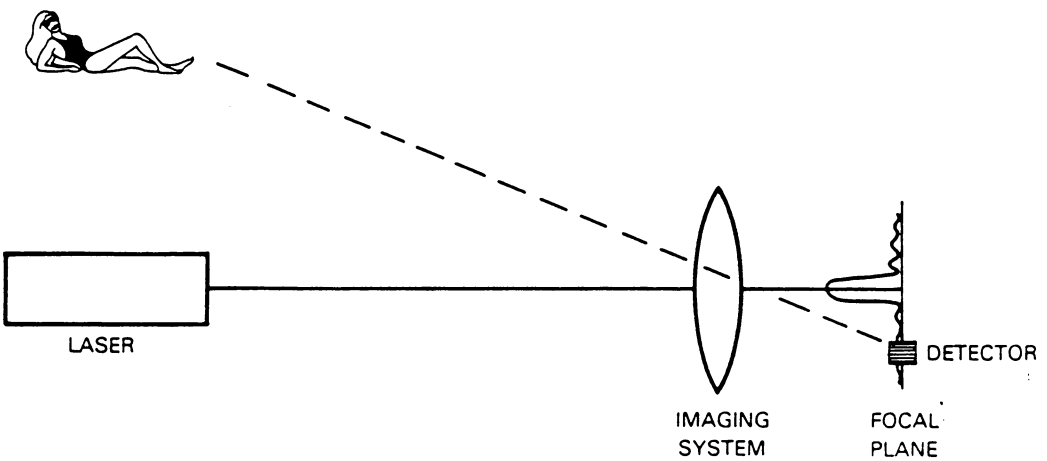

FIGURE 5.1 Detector corresponding to an off-axis position as the main diffraction pattern is formed in the center of the focal plane.

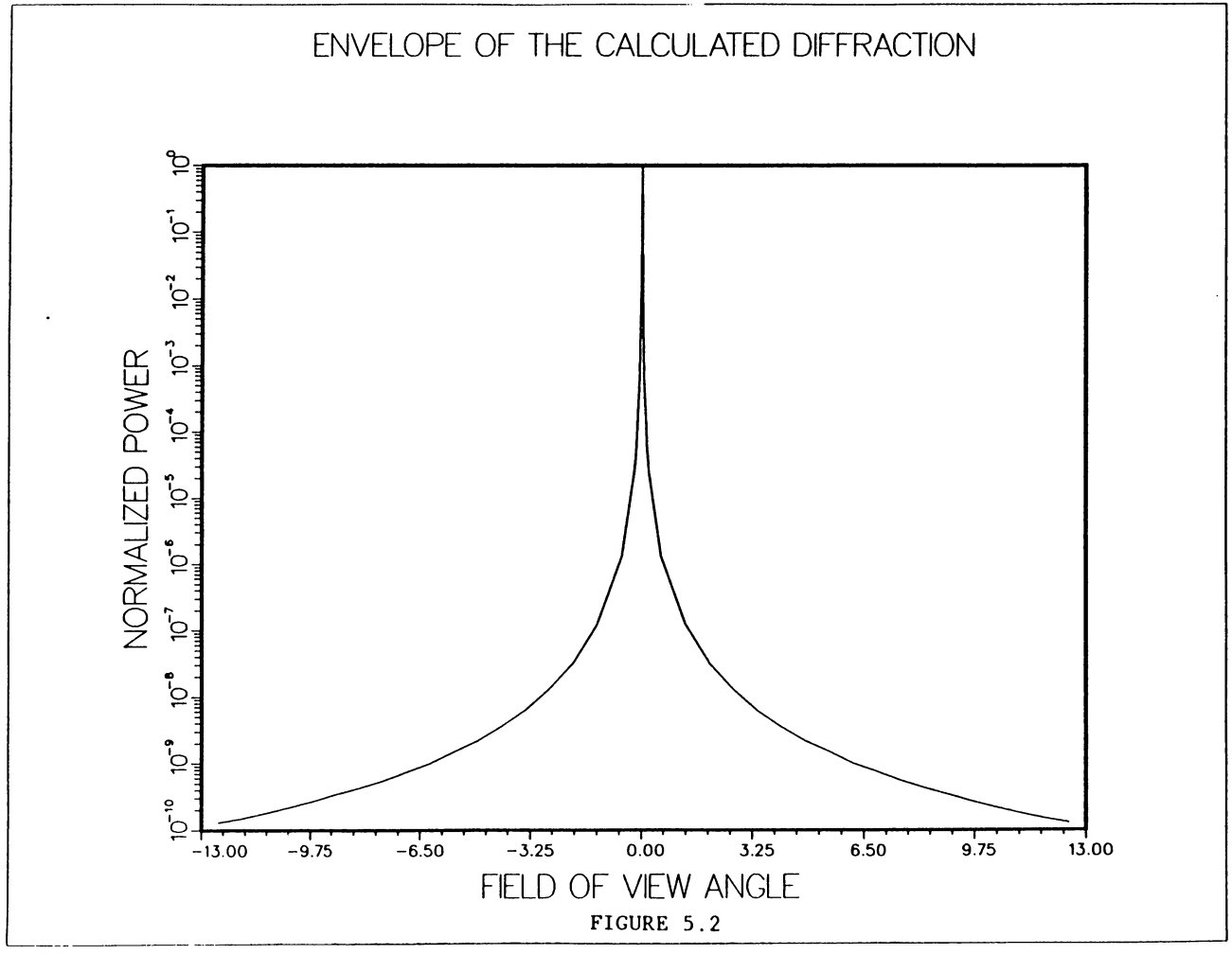
ENVELOPE OF THE CALCULATED DIFFRACTION
NORMALIZED POWER
10^{0}
10^{-1}
10^{-2}
10^{-3}
10^{-4}
10^{-5}
10^{-6}
10^{-7}
10^{-8}
10^{-9}
10^{-10}
-13.00
-9.75
-6.50
-3.25
0.00
3.25
6.50
9.75
13.00
FIELD OF VIEW ANGLE

FIGURE 5.2

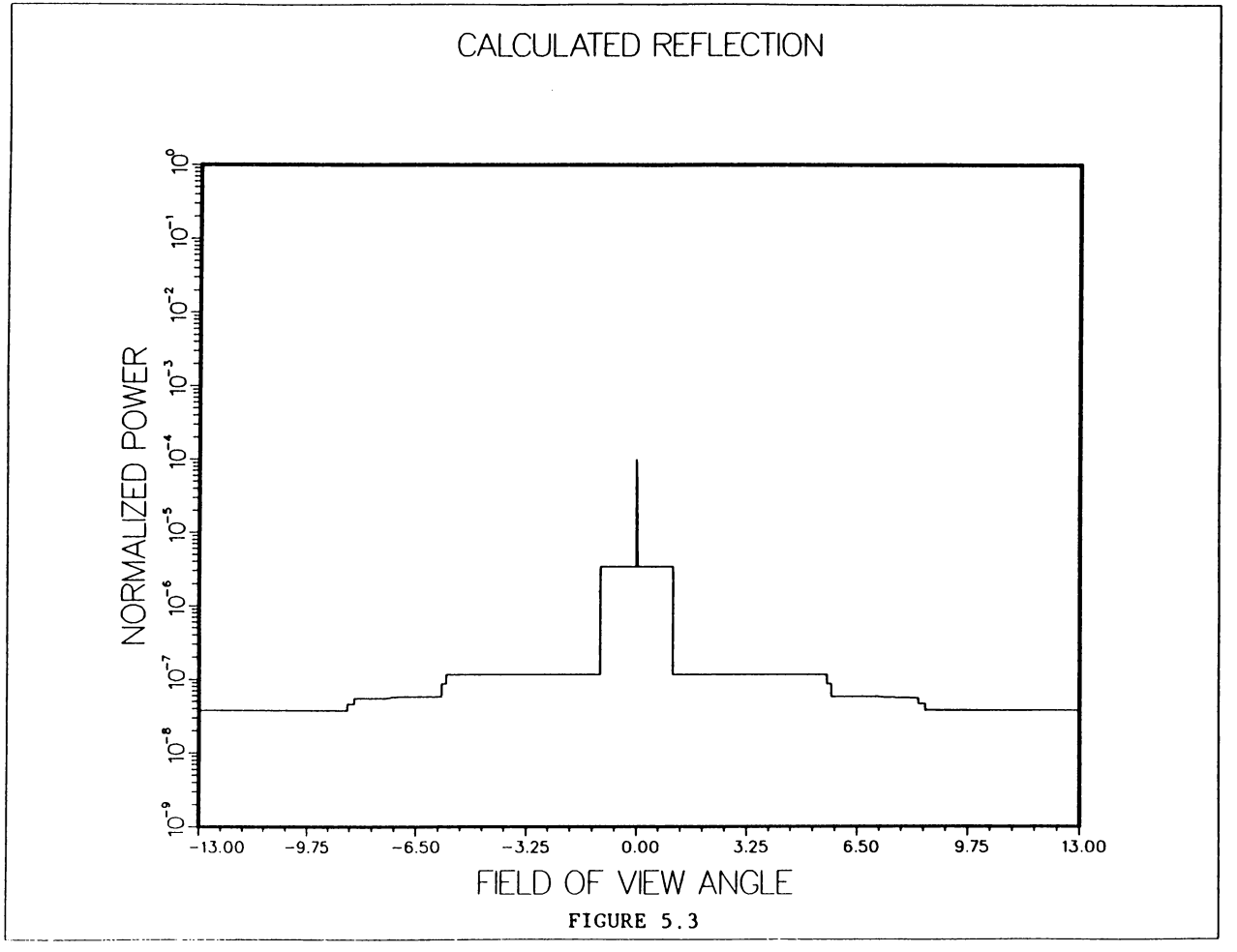
CALCULATED REFLECTION
NORMALIZED POWER
10^{0}
10^{-1}
10^{-2}
10^{-3}
10^{-4}
10^{-5}
10^{-6}
10^{-7}
10^{-8}
10^{-9}
-13.00
-9.75
-6.50
-3.25
0.00
3.25
6.50
9.75
13.00
FIELD OF VIEW ANGLE

FIGURE 5.3

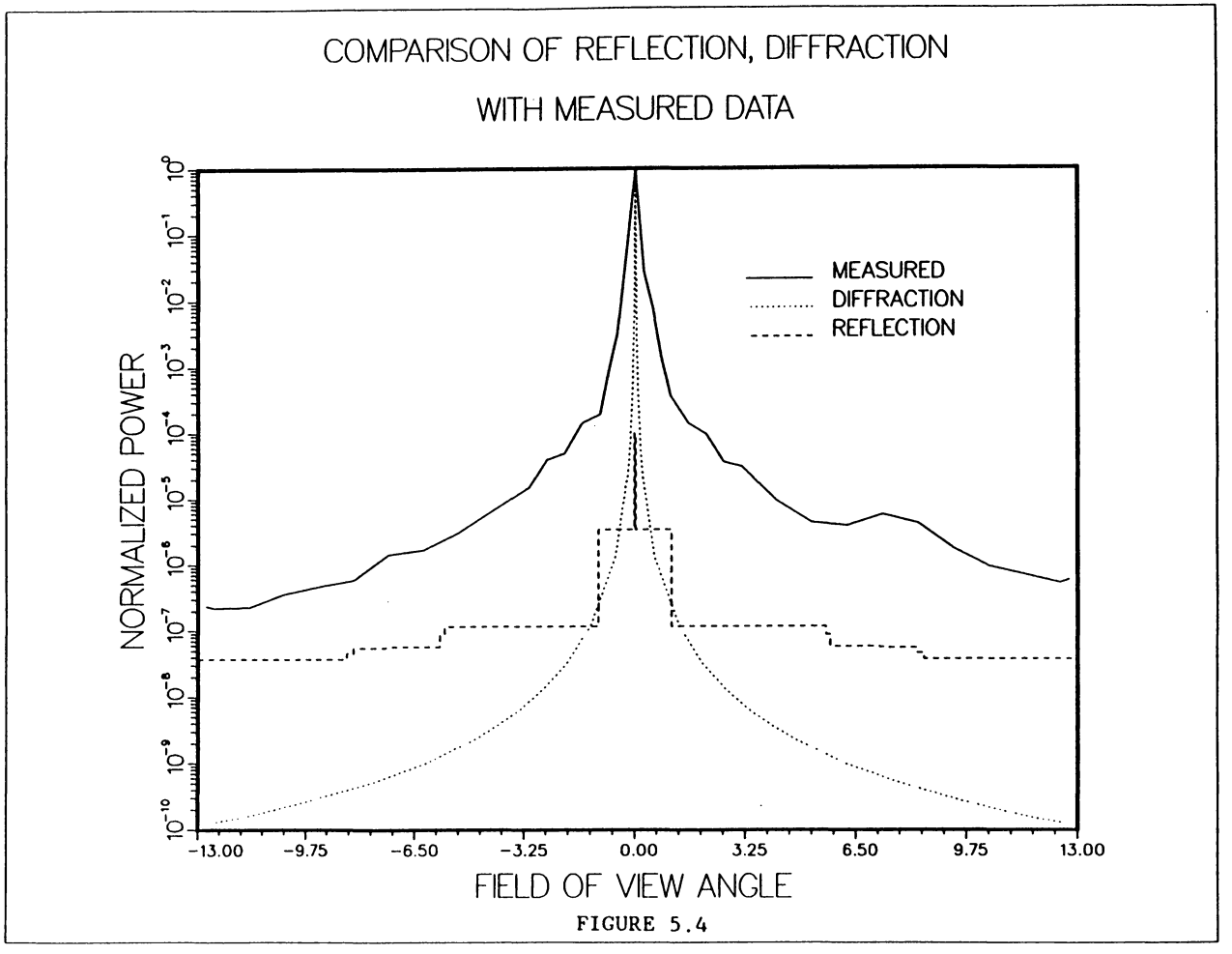
COMPARISON OF REFLECTION, DIFFRACTION
WITH MEASURED DATA
NORMALIZED POWER
10^{0}
10^{-1}
10^{-2}
10^{-3}
10^{-4}
10^{-5}
10^{-6}
10^{-7}
10^{-8}
10^{-9}
10^{-10}
MEASURED
DIFFRACTION
REFLECTION
-13.00
-9.75
-6.50
-3.25
0.00
3.25
6.50
9.75
13.00
FIELD OF VIEW ANGLE

FIGURE 5.4

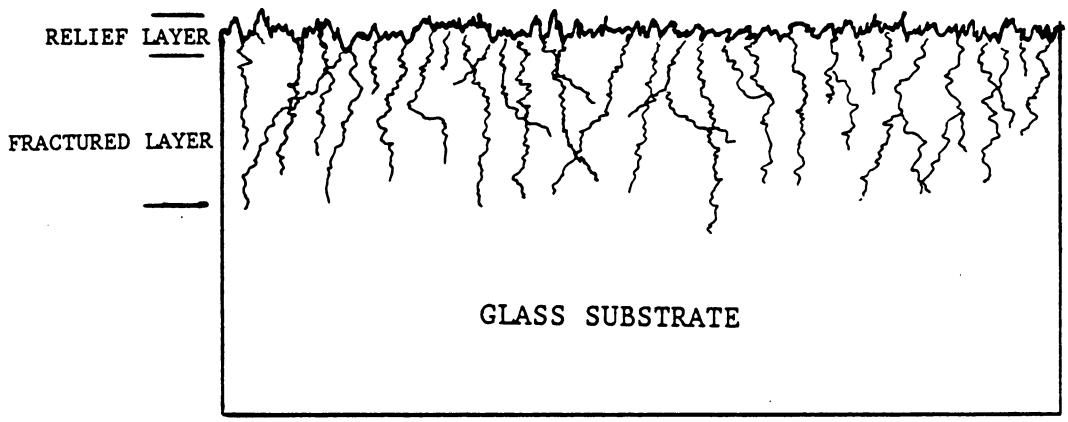

FIGURE 5.5 Section of ground glass surface showing the fractured and relief layers.

APPENDIX

Plane wave diffraction through a circular aperture

The intensity of the Fraunhoffer diffraction pattern from a circular aperture is described by equation (5.1.1). The entrance aperture of the our imaging system has a radius of 2.11 cm and is 8.4 cm from the focal plane, which gives a maximum Bessel Function argument of 3275. The Bessel Function can be approximated for large arguments* using

$$J_1(z) \doteq \sqrt{\frac{2}{\pi z}} \left[\cos\left\{ z - \frac{3\pi}{4} \right\} \sum_{m=0}^{\infty} \frac{(-1)^m (1,2m)}{(2z)^{2m}} - \sin\left\{ z - \frac{3\pi}{4} \right\} \sum_{m=0}^{\infty} \frac{(-1)^m (1,2m+1)}{(2z)^{2m+1}} \right]$$

where $$(1,m) = \frac{\Gamma(3/2 + m)}{m!\,\Gamma(3/2 - m)}$$

As the Bessel Function argument gets large, the first summation approaches unity, and the second summation approaches zero due to inverse powers of z. The first term for the cosine and sine summations are 1 and $3/8z$ respectively. With an argument of z=50, the terms are 1 and .0075. Thus an error of less than one percent has been introduced by neglecting higher order terms for large arguments. If the envelope of the diffraction pattern is desirable, as a worst case, then the cosine function is set to unity. The intensity of the diffraction pattern for large arguments becomes:

$$I(r) = I_o\left[\frac{8}{\pi(ka\omega)^3}\right]$$

where $z = ka\omega$ defined in eqn. (5.1.1).

The diffraction curve in figure 5.2 was plotted with this equation for Bessel function arguments larger than fifty. Tabulated data† was used for smaller arguments.

---

* G. S. Watson, *A Treatise os the Theory of Bessel Functions, Second Ed.*, The University Press, Cambridge, 1944.

† Howard H. Aiken, Tech. Dir., *Tables of Bessel Functions of the First Kind of orders Zero and One*, Harvard University Press, Cambridge, 1947.

REFERENCES

[1] P. C. Archibald and H. E. Bennett, "Scattering from Infrared Missle Domes", Opt. Eng., vol. 17, no. 6, pp.647-651, 1978.

[2] J. M. Elson and H. E. Bennett, "Image degredation caused by direct scatter from optical components into the image plane", Proc. SPIE, vol.511, pp. 7-11, 1984.

[3] Allen Nussbaum and Richard A. Phillips, *Contemporary Optics for Scientists and Engineers*, New Jersey: Prentice-Hall, Inc., 1976, p. 221.

[4] Eugine Hecht and Alfred Zajac, *Optics*, Massachusettes: Addison-Wesley Publishing Company, 1974, ch. 10.

[5] G. P. Agrawal and M. Lax, "Fraunhofer diffraction in the beam approximation from two longitudinally separated slits", J. Opt. Soc. Am., vol. 72, no.1, pp. 164-66, 1982.

[6] L. P. Boivin, "Diffraction corrections in radiometry: comparison of two different methods of calculation", Appl. Opt., vol.14, no. 8, pp. 2002-2009, 1975.

[7] For example: Alan W. Greynolds, "Methods for calculating diffraction effects in opto-mechanical systems of arbitrary geometry", Proc. SPIE, vol. 257, pp.64-77, 1980.

[8] Max Born and Emil Wolf, *Principles of Optics*, New York: Pergamon Press, 1980, p 40.

[9] W. L. Wolf and G. J. Zissis, ed., *The Infrared Handbook*, Environmental Research Institute of Michigan, 1985, ch. 7.

[10] Martin G. Schinker and Walter Doll, "Basic Investigations into the High Speed Processing of Optical Glasses with Diamond Tools", Proc. SPIE, vol. 381, pp.32-38, 1983.

[11] L. S. Tsesnek, "Physical laws of abrasive disintegration", *Generation of Optical Surfaces*, London: The Focal Library, 1962, pp. 419-436.

[12] V. M. Vinokurov, A. L. Ardamatskii and L. V. Popov, "The Structure of the Disrupted Layer", *Generation of Optical Surfaces*, London: The Focal Library, 1962, pp. 15-66.

[13] H. E. Bennett and M. J. Soileau, "Fabricating Infrared Optics", Opt. Eng., vol. 15, no. 5, pp. 442-445, 1976.

[14] John C. Stover, "Surface characteristics of machined optics", Proc. SPIE, vol. 93, pp. 90-95, 1976.

[15] John C. Stover, "Roughness characterization of smooth machined surfaces by light scattering", Appl. Opt., vol. 14, no. 8, pp. 1796-1802, 1975.

[16] E. L. Church and J. M. Zavada, "Residual surface roughness of diamond-turned optics", Appl. Opt., vol. 14, no. 8, pp. 1788-1795, 1975.

[17] Jean M. Bennett, "Comparison of techniques for measuring the roughness of optical surfaces", Opt. Eng., vol. 24, no. 3, pp. 380-387, 1985.

[18] J. M. Elson and J. M. Bennett, "Relation between the angular dependence of scattering and the statistical properties of optical surfaces", J. Opt. Soc. Am., vol. 69, no. 1, pp. 31-47, 1979.

[19] F. O. Bartell, E. L. Dereniak and W. L. Wolf, "The Theory and measurement of bidirectional reflectance distribution function (BRDF) and bidirectional transmittance distribution function (BTDF)", Proc. SPIE, vol. 257, pp. 154-160, 1980.

[20] Karl H. Guenther, Peter G. Wierner, and Jean M. Bennett, "Surface roughness measurements of low-scatter mirrors and roughness standards", Appl. Opt., vol. 23, no. 21, pp. 3820-3836, 1984.

[21] John C. Stover and Steven A. Serati, "Calculation of surface statistics from light scatter", Proc. SPIE, vol. 429, pp. 96-104, 1983.

[22] R. P. Young, "Low-Scatter Mirror Degredation by Particle Contamination", Opt. Eng., vol. 15, no. 6, pp. 516-520, 1976.

[23] V. A. Gogolev, I. A. Zabelina, V. N. Rogova, and S. L. Shaiovich, "Photometric characteristics of contaminated flat optical components", Sov. J. Opt. Tech., vol. 47, no. 10, pp. 576-578, 1980.

[24] Yaujen Wang, "Scattering from mirrors contaminated by particulates: a model", Appl. Opt., vol. 25, no. 23, pp. 4222-4223, 1986.

[25] For example: R. J. Noll, P. E. Glenn and J. Osantowski, "Optical surface analysis code (OSAC)", Proc. SPIE, vol.362, pp. 78-85, 1982.

[26] Janet S. Fender, "Stray radiation analysis programs (GUERAP III - APART/PADE): a user's viewpoint", Proc. SPIE, vol. 257, pp. 94-103, 1980.

The vita has been removed from the scanned document